International Journal of Heat and Mass Transfer 51 (2008) 5877–5886

Contents lists available at ScienceDirect

International Journal of Heat and Mass Transfer

journal homepage: www.elsevier.com/locate/ijhmt

Dendritic vascularization for countering intense heating from the side

S. Kim [a], S. Lorente [b], A. Bejan [a,*]

[a] Department of Mechanical Engineering and Materials Science, Duke University, Durham, NC 27708-0300, USA
[b] Laboratoire Matériaux et Durabilité des Constructions, Département de Génie Civil, Institut National des Sciences Appliquées, 135 Avenue de Rangueil, 31077 Toulouse, France

ARTICLE INFO

Article history:
Received 3 January 2008
Received in revised form 30 April 2008
Available online 14 July 2008

Keywords:
Constructal
Vascularized
Turbine blade cooling
Dendritic
Volumetric cooling
Svelteness

ABSTRACT

This paper is a proposal to vascularize a solid wall with transverse tree-shaped channels with fluid flow from side to side. The purpose of the fluid flow is to intercept in counterflow the solid heat conduction caused by an intense heat flux that lands on the exit plane of the wall. Tree architectures with 1–4 levels of bifurcation are simulated numerically, as a conjugate (convection and conduction) heat flow phenomenon in three dimensions. The effect of local pressure losses at junctions and entrances is included. The numerical work covers the Reynolds number range 10–550, svelteness number range 2.2–11.5, wall porosity range 0.01–0.1, and pressure drop number range 3×10^5–10^{10}. The objective of the tree flow is to keep down the peaks of hot spot temperatures and the fraction of the volume occupied by high temperatures while using minimum pumping power. It is shown that the tree design is very effective, and that there is an optimal number of bifurcation levels for a specified porosity and pressure drop number. Tree designs are more effective than designs with parallel channels when the pressure drop number and the porosity are sufficiently large.

1. The vascularization revolution

Heat transfer has undergone several "revolutions" before becoming classical in both education and practice. Noteworthy examples (new waves at the time) are (i) convection, which was triggered by Prandtl's boundary layer theory 100 years ago, (ii) augmentation, which was stimulated by Bergles' organizing of a highly diverse arena of discovery, and (iii) miniaturization, which still goes on as a march toward micro- and nano-heat transfer configurations. The literature of the last decade is showing another change—a new page in the book of fundamentals. It is the development of tree-shaped flow architectures for applications that in the classical past relied on arrays of parallel channels (e.g., Fig. 1).

Tree-shaped vascularization is a significant change, because the use of parallel channels is intuitive, simple and very popular in engineering. And, contrary to the impression stemming from their widespread use in microscale design of electronics today, the parallel channels configuration is almost 200 years old. We inherited the idea and the textbook drawing from Seguin's 1829 invention of the locomotive boiler with a large number of parallel tubes.

Tree-shaped paths were proposed as necessary configurations for heat flow in 1996 [1,2]. The argument was that the miniaturization revolution will take the design of cooling configurations to

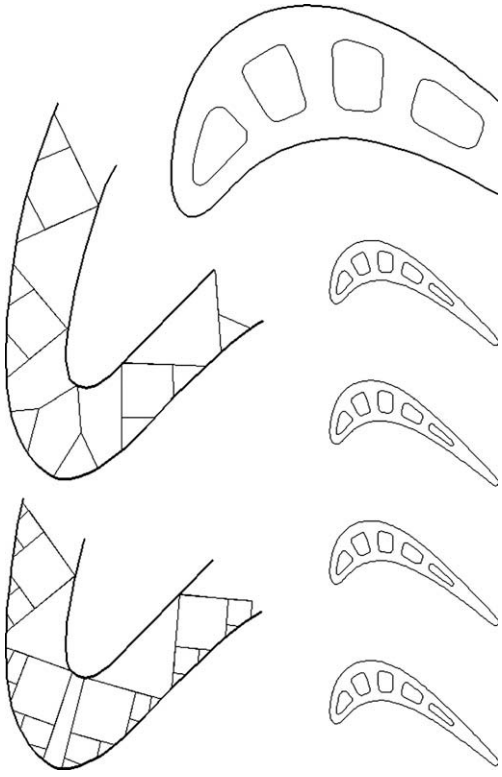

Fig. 1. Proposal to vascularize with tree-shaped flow structures the walls of turbine blades and other bodies exposed to intense heating [3].

* Corresponding author. Tel.: +1 919 660 5310; fax: +1 919 660 8963.
E-mail address: dalford@duke.edu (A. Bejan).

0017-9310/$ - see front matter © 2008 Elsevier Ltd. All rights reserved.
doi:10.1016/j.ijheatmasstransfer.2008.04.063

Nomenclature

A	area (m^2)
A_σ	hot-area (m^2)
Be	Bejan number, Eq. (23)
c_p	specific heat (J/kg K)
d	smallest length scale (m)
D_i	channel diameters (m)
k	thermal conductivity (W/m K)
$\tilde{k}$	ratio of thermal conductivities, Eq. (22)
L	length (m)
$\dot{m}$	mass flow rate (kg/s)
p	number of pairing levels
P	pressure (Pa)
Pr	Prandtl number, Eq. (22)
q''	heat flux (W/m^2)
Re_i	Reynolds numbers, U_iD_i/v
Sv	svelteness number, Eq. (24)
T	temperature (K)
$\widetilde{T}$	dimensionless excess temperature, Eq. (13)
T_σ	lowest temperature on the hot-area, Eq. (26)
u, v, w	velocity components (m/s)
U_i	mean velocities (m/s)
V	total volume (m^3)
V_c	total volume of channels (m^3)
$\dot{W}$	pumping power (W)
x, y, z	Cartesian coordinate axes

Greek letters

α	thermal diffusivity (m^2/s)
ΔP	pressure drop (Pa)
μ	viscosity (kg/s m)
v	kinematic viscosity (m^2/s)
ρ	density (kg/m^3)
σ	hot-area fraction, A_σ/A
ϕ	porosity, void fraction

Subscripts

f	fluid
in	inlet
max	maximum, hot spot
min	minimum
out	outlet
s	solid

scales so small that the cooling of every heat-generating subvolume becomes an area-point or volume-point flow problem. Constructal theory grew from this seed, and showed that the easiest way to flow from an infinite number of points (area, volume) to one point is to flow as a tree. Recent reviews [3,4] show that the field has grown at a fast pace, in several directions, and in independent groups of investigations. For example, trees were developed for convection on rectangular and disc-shaped bodies [5–12], fuel cells [13,14], heat exchangers [15–20], and smart materials with volumetric self-healing functionality [21–23].

The trend is toward finer (smaller scales) and more effective tree architectures. Beneficiaries are the new concepts of smart materials with new functionalities such as sensing, self-healing, variable (designed) local transport properties, volumetric chemical reactions, and high-density volumetric cooling. The focus of this paper is on the use of trees for cooling, specifically for fighting against intense heating from the side, as in thermal management of aircraft and cooling of turbine blades (Fig. 1) [3]. In Ref. [24], we showed that if we use parallel channels with flow oriented against the side heat flux, it is possible to select the internal vasculature of the flow system such that the solid body is protected most effectively against overheating.

In this paper, we propose to use tree-shaped flow architectures to prevent the overheating that would be caused by intense side heating, Fig. 1. The fundamental question is under what conditions is the configuration of Fig. 1 more effective than parallel channels with flow oriented against q''. The question is fundamental because it is relevant to vascularizing all sorts of solid walls that must be protected against overheating. When are the tree-shaped channels more effective than current designs, which employ parallel channels oriented across the wall? For simplicity, we consider this problem in the steady state.

2. Model

The vascularized wall has many elemental volumes of the kind shown in Fig. 2. The solid slab of thickness L is heated with uniform heat flux q'' from the left side. The right side is insulated. The slab is cooled by a single-phase fluid driven by a specified pressure difference, ΔP. In the example of Fig. 2 the number of pairing or bifurcation levels is $p = 3$. The volume element has one inlet on the right side, and 2^{p+1} outlets on the left side. All the channels are round, and the diameters of the channels are sized relative to one another in accordance with the Hess–Murray law [3,25],

$$D_i/D_{i+1} = 2^{1/3}, \quad i = 1, 2, \ldots, p \tag{1}$$

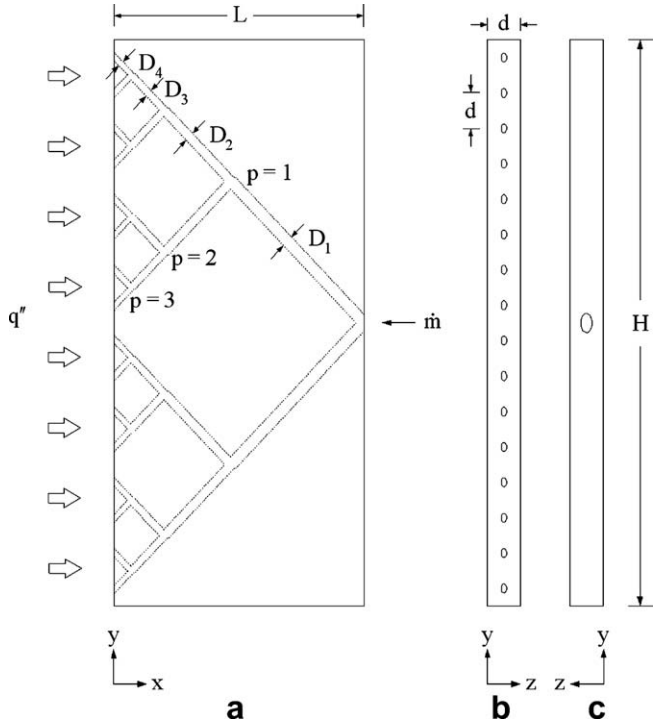

Fig. 2. Tree-shaped flow structure with three levels of bifurcation: (a) the mid plane of the flow element; (b) the view from the left, showing the outlets; (c) the view from the right, showing the inlet.

The thickness of the element in the direction perpendicular to the figure is set equal to the spacing (d). The vertical dimension H of the element is $2^{p+1}d$. Several volume elements stacked in the vertical direction in Fig. 2 constitute a slab vascularized with line-to-line tree structures.

The configuration of a single tree is based on the minimal-length method proposed in Ref. [26]. This is an approximate method of constructing near-optimal trees, and its use in this work is recommended by its simplicity and accuracy. The simplicity is that the bifurcations turn out to have 90° angles, which make the outer channels be collinear. The accuracy is surprisingly good, for example, the global flow resistance of a minimal-length Y-shaped structure exceeds by only 0.5% the global resistance of a fully optimized Y construct [27]. The bifurcation angles of the fully optimized Y construct are also comparable with the angles shown in Fig. 2.

3. Numerical simulations

To evaluate the performance of the tree vasculature, we simulated the flow and temperature fields as a conjugate (conduction and convection) heat transfer steady state, by using a finite volume CFD code [28]. The conservation equations for mass and momentum in the flow spaces are

$$\frac{\partial u}{\partial x}+\frac{\partial v}{\partial y}+\frac{\partial w}{\partial z}=0 \tag{2}$$

$$\rho\left(u\frac{\partial u}{\partial x}+v\frac{\partial u}{\partial y}+w\frac{\partial u}{\partial z}\right)=-\frac{\partial P}{\partial x}+\mu\nabla^2 u \tag{3}$$

$$\rho\left(u\frac{\partial v}{\partial x}+v\frac{\partial v}{\partial y}+w\frac{\partial v}{\partial z}\right)=-\frac{\partial P}{\partial y}+\mu\nabla^2 v \tag{4}$$

$$\rho\left(u\frac{\partial w}{\partial x}+v\frac{\partial w}{\partial y}+w\frac{\partial w}{\partial z}\right)=-\frac{\partial P}{\partial z}+\mu\nabla^2 w \tag{5}$$

where $\nabla^2 = \partial^2/\partial x^2 + \partial^2/\partial y^2 + \partial^2/\partial z^2$. Energy conservation in the fluid and solid spaces is expressed by

$$(\rho c_p)_{\mathrm{f}}\left(u\frac{\partial T}{\partial x}+v\frac{\partial T}{\partial y}+w\frac{\partial T}{\partial z}\right)=k_{\mathrm{f}}\nabla^2 T \tag{6}$$

$$\nabla^2 T=0 \tag{7}$$

The heat flux imposed from the side is

$$q''=-k_{\mathrm{s}}\frac{\partial T}{\partial x} \tag{8}$$

The continuity of heat flux across the solid–fluid interfaces is expressed by

$$k_{\mathrm{s}}\frac{\partial T}{\partial n}=k_{\mathrm{f}}\frac{\partial T}{\partial n} \tag{9}$$

where n is the direction normal to the surface. For greater generality, we determined the flow and temperature fields in dimensionless form by using the variables

$$(\tilde{x},\tilde{y},\tilde{z},\tilde{n})=(x,y,z,n)/L \tag{10}$$

$$(\tilde{u},\tilde{v},\tilde{w})=(u,v,w)L/\alpha_{\mathrm{f}} \tag{11}$$

$$\widetilde{P}=(P-P_{\mathrm{out}})L^2/(\mu\alpha_{\mathrm{f}}) \tag{12}$$

$$\widetilde{T}=(T-T_{\mathrm{min}})k_{\mathrm{s}}/(q''L) \tag{13}$$

where P_{out} is the lowest pressure (at the outlets), and T_{min} is the inlet temperature of the coolant. Written in terms of dimensionless variables, Eqs. (2)–(9) become

$$\frac{\partial\tilde{u}}{\partial\tilde{x}}+\frac{\partial\tilde{v}}{\partial\tilde{y}}+\frac{\partial\tilde{w}}{\partial\tilde{z}}=0 \tag{14}$$

$$\frac{1}{Pr}\left(\tilde{u}\frac{\partial\tilde{u}}{\partial\tilde{x}}+\tilde{v}\frac{\partial\tilde{u}}{\partial\tilde{y}}+\tilde{w}\frac{\partial\tilde{u}}{\partial\tilde{z}}\right)=-\frac{\partial\widetilde{P}}{\partial\tilde{x}}+\nabla^2\tilde{u} \tag{15}$$

$$\frac{1}{Pr}\left(\tilde{u}\frac{\partial\tilde{v}}{\partial\tilde{x}}+\tilde{v}\frac{\partial\tilde{v}}{\partial\tilde{y}}+\tilde{w}\frac{\partial\tilde{v}}{\partial\tilde{z}}\right)=-\frac{\partial\widetilde{P}}{\partial\tilde{y}}+\nabla^2\tilde{v} \tag{16}$$

$$\frac{1}{Pr}\left(\tilde{u}\frac{\partial\tilde{w}}{\partial\tilde{x}}+\tilde{v}\frac{\partial\tilde{w}}{\partial\tilde{y}}+\tilde{w}\frac{\partial\tilde{w}}{\partial\tilde{z}}\right)=-\frac{\partial\widetilde{P}}{\partial\tilde{z}}+\nabla^2\tilde{w} \tag{17}$$

$$\tilde{u}\frac{\partial\widetilde{T}}{\partial\tilde{x}}+\tilde{v}\frac{\partial\widetilde{T}}{\partial\tilde{y}}+\tilde{w}\frac{\partial\widetilde{T}}{\partial\tilde{z}}=\nabla^2\widetilde{T} \tag{18}$$

$$\nabla^2\widetilde{T}=0 \tag{19}$$

$$1=-\frac{\partial\widetilde{T}}{\partial\tilde{x}} \tag{20}$$

$$\tilde{k}\left.\frac{\partial\widetilde{T}}{\partial\tilde{n}}\right|_{\mathrm{s}}=\left.\frac{\partial\widetilde{T}}{\partial\tilde{n}}\right|_{\mathrm{f}} \tag{21}$$

where the dimensionless groups are

$$Pr=\frac{\nu}{\alpha_{\mathrm{f}}},\quad \tilde{k}=\frac{k_{\mathrm{s}}}{k_{\mathrm{f}}} \tag{22}$$

The imposed pressure difference ΔP gives rise to another dimensionless group,

$$Be=\frac{\Delta PL^2}{\mu\alpha_{\mathrm{f}}} \tag{23}$$

which is the pressure drop Bejan number proposed in Refs. [29,30]. The Be value is fixed because ΔP is fixed. Note that this group is the same as the dimensionless inlet excess pressure $\widetilde{P}$ defined in Eq. (12). The dimensionless conjugate heat transfer was solved with segregated solid energy solver and the segregated fluid flow and temperature solvers that the CFD code [28] provides. The convection terms were discretized using the second order upwind scheme with the secondary gradient option being enabled. An algebraic multigrid (AMG) algorithm was used to solve the linear matrices.

The numerical simulations were conducted in the nondimensional parametric domain represented by $Pr = 6$, $\tilde{k} = 30$, and $Be = 10^6$–10^{10}. The volume fraction (or porosity ϕ) occupied by all the channels was set at 0.05. For example, the pressure drop is in the range 1.3–1.3 × 10^4 Pa, and the hot spot (excess temperature) in the range 304–410 K when $T_{\mathrm{min}} = 300$ K, $L = 0.01$ m, $q'' = 10^5$ W/m^2, and the solid is stainless steel and the fluid is liquid water.

The resulting flow rates were such that the Reynolds numbers based on channel diameters ($Re_i = U_i D_i/\nu$) were less than 10^3. These parameters are the same as in an earlier study of parallel channels across the wall [24], and justify the comparison between trees and parallel channels.

The objective of the simulations was to determine the effect of the tree architecture design on the temperature field in the vascularized volume. The temperature distribution will always be nonuniform. The search is for designs that depress the temperature peaks (the hot spots) to the lowest levels possible. The question is whether tree-shaped architectures maintain a relatively more uniform temperature distribution than parallel channels.

Tree configurations for convection have been studied originally by assuming fully developed laminar flow in all the channels. Junction and entrance losses become nonnegligible when the channels are short and numerous. It was shown that the effect of junction losses cannot be neglected when the global geometric property (the svelteness number [31])

$$Sv = \frac{\text{external flow length scale}}{\text{internal flow length scale}} = \frac{L}{V_c^{1/3}} \quad (24)$$

is less than the order of 10. In the $Sv < 10$ domain, full numerical simulations of the flow near every junction and corner are necessary. This is the method used in the present study. The total flow volume V_c and corresponding porosity ($\phi = 0.01$–0.1) were such that Sv was in the range 2.2–11.5.

It is worth noting that the svelteness is a global property of the entire tree flow architecture, not the slenderness of one of the channels. The tree has many channels, each with its own, optimal, L/D ratio. And even when there is only one flow feature (one channel) in the drawing (as in arrays of parallel channels), the slenderness of the channel (L/D) is not the same as the svelteness of the drawing, $Sv \sim L/(D^2L)^{1/3} \sim (L/D)^{2/3}$. Svelteness is a global property of the entire drawing, that is the flow channels and their background (interstices), while slenderness is a property of a single channel. The merit of the Sv concept stems from the fact that it describes the entire flow architecture, and that it tells when the architecture as a whole suffers from nonnegligible junction losses [31].

Another flow feature that becomes accentuated when $Sv < 10$ is the nonuniformity of the flow rates through channels of the same rank. The nonuniformity is due to the asymmetry of each Y-shaped construct: because of inertia, more fluid flows along the straight (continuation) channel downstream from every bifurcation. The important development that we report here is that flow-splitting asymmetry is actually beneficial for the purpose of making the temperature field more uniform. Flow asymmetry places the larger flow rates in the outer channels, and it is here, around the outer channels that the conducting solid has relatively less vascularization and tends to overheat.

Because Sv was not large, junction losses were important: their presence is illustrated in Fig. 3 for a tree structure with three bifurcation levels, $\phi = 0.05$ and $Be = 10^9$ ($Sv = 5.2$). Because of the asymmetric Y-shaped junctions, significant pressure losses occur at the junctions, especially when the flow makes a 90° turn. Flow nonuniformity is another result of the turns. Compare, for example, the flow rates downstream of junction A, namely $\dot{m}_2/\dot{m}'_2 = 0.59/0.41 = 1.44$. Similar flow imbalances occur downstream of junctions B and C, where $\dot{m}_3/\dot{m}'_3 = 1.42$ and $\dot{m}_4/\dot{m}'_4 = 1.59$, respectively.

How the tree architecture shaves the hot spots is illustrated by the $p = 4$ structure shown in Fig. 4. This is the temperature distribution in the mid plane of the slab. The hot spots occur in the two extreme corners of the tree canopy. The tree-shaped flow intercepts the heat flux, and prevents it from advancing by conduction toward the right side of the slab.

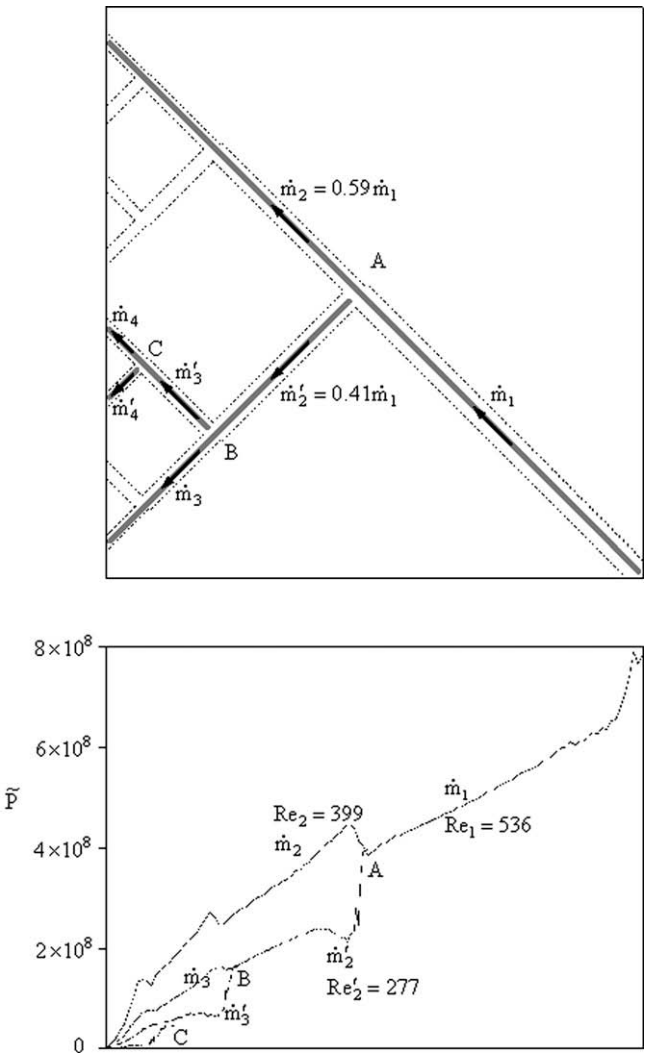

Fig. 3. Pressure distribution and mass flow rates along the channels of a tree with $p = 3$, $\phi = 0.05$ ($Sv = 5.2$) and $Be = 10^9$.

4. Trees versus parallel channels

The following is a systematic presentation of the results, from the simplest to the more complex architectures. Fig. 5 and Table 1 report the hot spot temperatures in the design with one bifurcation level. The construction of the dimensionless group used on the ordinate of Fig. 5 is recommended by the scale analysis for cooling with parallel channels [24]. The dashed-line shows that the hot spots become colder as the applied pressure difference and the resulting flow rates increase. The log–log relation between $\tilde{T}_{max}$ and Be is not a straight line. This finding differs from the solid line drawn for parallel channels, which is nearly straight. The reason why the two lines differ is that the line for parallel channels represents the locus of configurations with optimized spacings. The performance curve for a single configuration with fixed (assumed) parallel channels spacing is a curve with positive curvature, which is tangent to the solid line [24]. Such a curve (not shown) would be analogous to the dashed curve drawn here for the tree structure, because the tree structure is assumed, i.e., it is not optimized beyond the minimal-length design of Ref. [26]. Said another way, the solid line is the envelope (the locus of the best designs) of the curves that could be drawn for parallel channels with assumed spacings. Along the solid line, the optimized channel spacing varies [24].

We used this idea and continued the study by constructing the envelope for the dashed curves of the tree structures. We did this by varying the number of pairing levels, p. The results are projected as solid lines in Fig. 6. Each constant-p curve is similar to the $p = 1$ curve shown in Fig. 5. Svelteness varies from 2.8 (at $p = 1$) to 6.7 (at $p = 4$). The envelope of the curves is a straight line, which is plotted with dashed-line. The envelope suggests that lower $\tilde{T}_{max}$ levels are achievable not only with more pressure (Be) but also with a higher p, i.e., with more complex tree architectures.

The dashed-line envelope of Fig. 6 has been added projected in Fig. 7 on top of the envelope for parallel channels with optimized spacings. The two lines intersect at approximately $Be \cong 3 \times 10^7$. When the specified pressure difference is such that $Be \geqslant 3 \times 10^7$, tree-shaped designs promise lower $\tilde{T}_{max}$ values than parallel channels. In order to derive maximum benefit from using trees, however, an optimal pairing level should be selected at a given pressure difference. The pairing level is marked with circles on

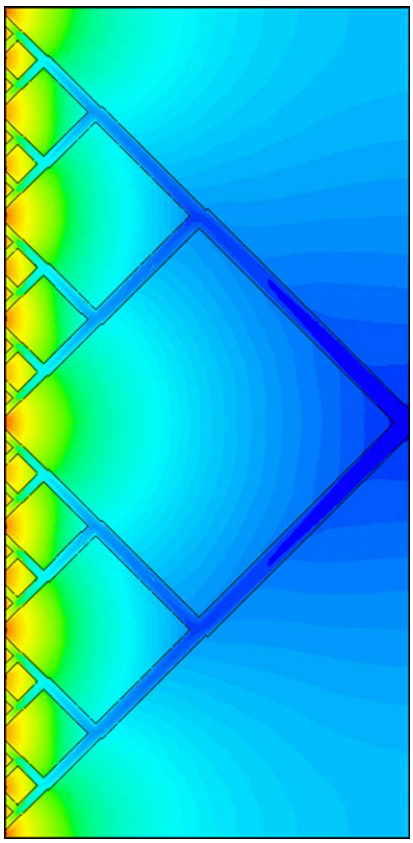

Fig. 4. Example of temperature distribution in the mid plane of a design with four levels of bifurcation ($\phi = 0.05$, $Be = 3 \times 10^8$).

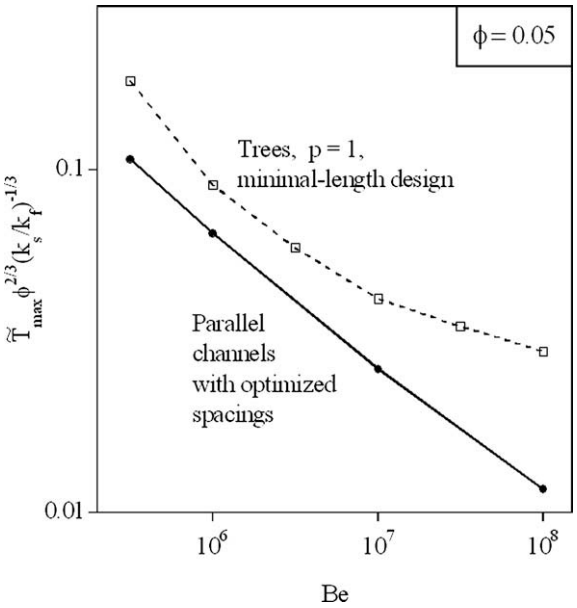

Fig. 5. The overall temperature differences $\tilde{T}_{max}$ for two designs: trees with one bifurcation level and parallel channels with optimized spacings.

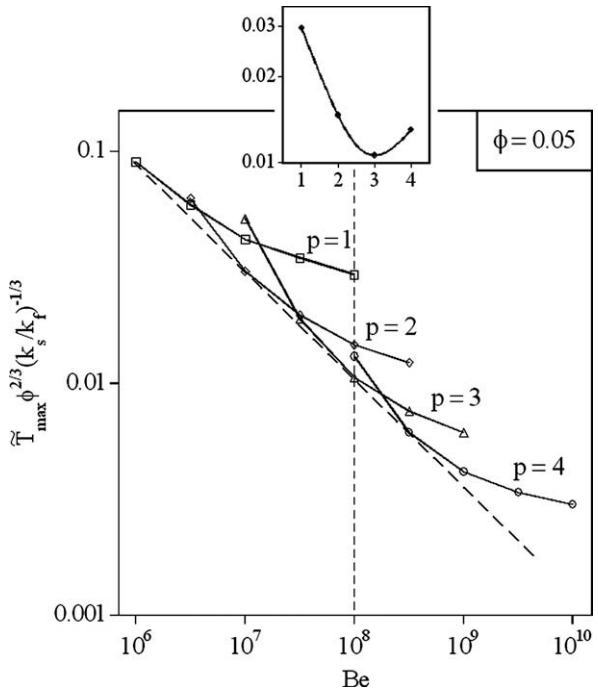

Fig. 6. The envelope of the hot spot curves for tree structures with $p = 1,\ldots,4$, and $\phi = 0.05$.

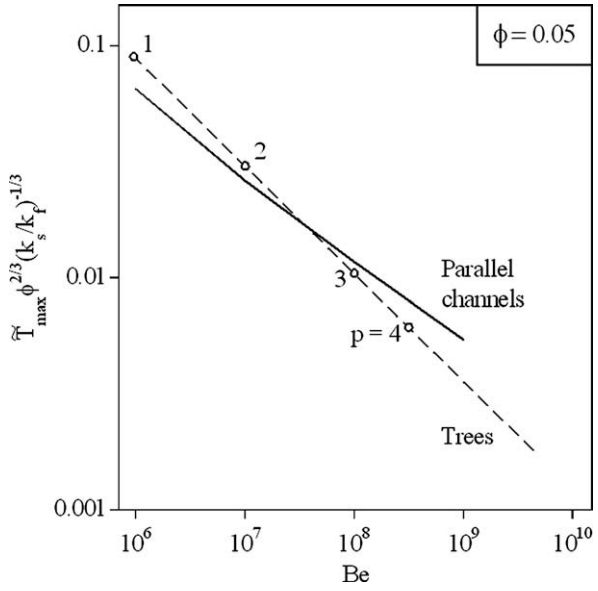

Fig. 7. Summary of the best designs with trees and parallel channels with optimized spacings and $\phi = 0.05$.

the dashed-line envelope. For example, the upper detail in Fig. 6 shows that when $Be = 10^8$ the best tree configuration has three pairing levels. The same conclusion is derived from Table 2 and Fig. 8. Table 2 shows that when $Be = 10^8$ a tree design with three

Table 1
The overall temperature difference $\tilde{T}_{max}$ for trees with one bifurcation level and for parallel channels with optimized spacings

Configurations	$Be = 3 \times 10^5$	$Be = 10^6$	$Be = 3 \times 10^6$	$Be = 10^7$	$Be = 3 \times 10^7$	$Be = 10^8$
Tree channels	4.164	2.068	1.358	0.962	0.800	0.677
Parallel channels	2.459	1.494	–	0.601	–	0.269

Table 2
The overall temperature difference $\tilde{T}_{max}$ for tree-shaped structures and parallel channels with optimized spacings

Be	Parallel	Trees, $p = 1$	Trees, $p = 2$	Trees, $p = 3$	Trees, $p = 4$
10^6	1.494	2.068			
10^7	0.601	0.962	0.700	1.182	
10^8	0.269	0.677	0.337	0.244	0.299
10^9	0.124			0.141	0.095

pairing levels improves by 9% the performance of parallel channels, but that the tree designs with $p = 1$, 2, and 4 are inferior to parallel channels with optimized spacings. The color illustrations in Fig. 8 show the temperature distributions in the bottom plane of the slab and the pressure distributions in the mid plane of the channels. Trees with $p = 3$ perform better because in this case the temperature distribution has least red area, i.e. least hot-area.

5. The effect of porosity

The porosity is an important architectural and mechanical strength feature that was held fixed at $\phi = 0.05$ in the designs of Figs. 5–8. We investigated the effect of porosity by repeating the work of Figs. 5–8 for three additional porosities, $\phi = 0.1$, 0.02, and 0.01. The thermal performance of trees with $\phi = 0.02$ is reported in Fig. 9. The curves and their dashed-line envelope are similar to what we showed in Fig. 6, but their position on the graph is different.

Fig. 10 compares the dashed-line envelope of Fig. 9 with the envelope for parallel channels with optimized spacings and $\phi = 0.02$. This figure is similar to Fig. 7, however, the intersection of the two envelopes occurs now at $Be \cong 4 \times 10^8$. In other words, when ϕ decreases the intersection of the envelopes shifts to a higher *Be* value, and to a higher *p* value for the tree design that lies on the envelope at the intersection.

The corresponding results for $\phi = 0.1$ and 0.01 are not shown because they are qualitatively the same as in Figs. 7 and 10. The

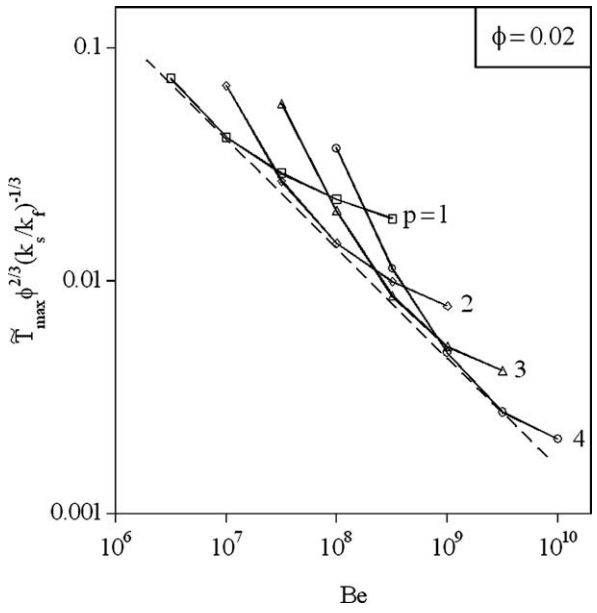

Fig. 9. The envelope of the hot spot curves for tree structures with $\phi = 0.02$.

points (ϕ, Be) where tree designs and parallel channels compete on an equal basis are reported in Fig. 11, along with the intersections viewed in Figs. 7 and 10. These points are indicated with circles, and trace a nearly straight line ($\phi \cong 40 Be^{-0.4}$) that divides the design space (ϕ, Be) into two domains. Parallel channels offer lower $\tilde{T}_{max}$ values when the design (ϕ, Be) falls below the line. Tree-shaped designs are preferable above the line. The dashed lines indicate the bands of tree designs (p) that fill the (ϕ, Be) space. The intersections of the dashed lines with the solid line indicate the complexity (p) of the trees that perform as well as the parallel channels when *Be* (or ϕ) is specified.

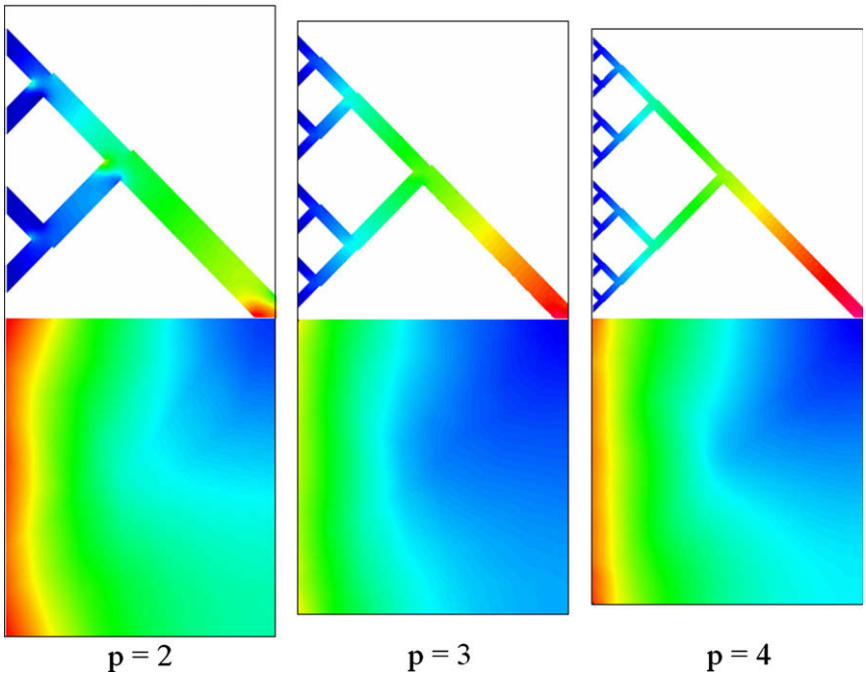

Fig. 8. The temperature distribution in the bottom plane and the pressure distribution in the mid plane of trees with $p = 2$, 3, and 4 ($\phi = 0.05$, $Be = 10^8$).

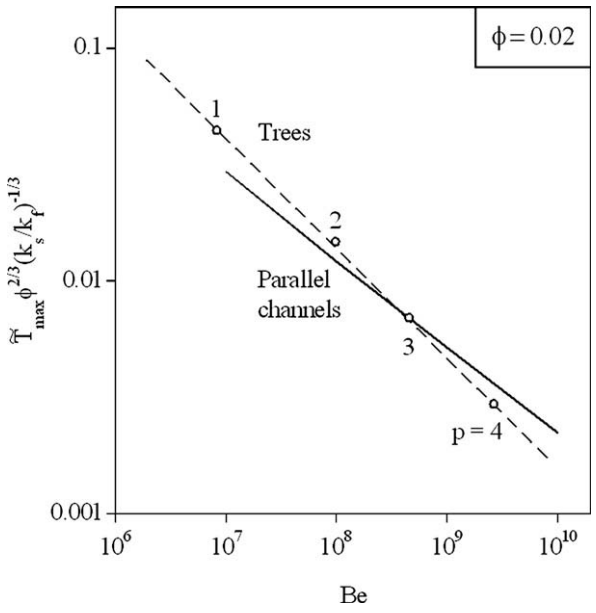

Fig. 10. Summary of the best designs with trees and parallel channels with optimized spacings and $\phi = 0.02$.

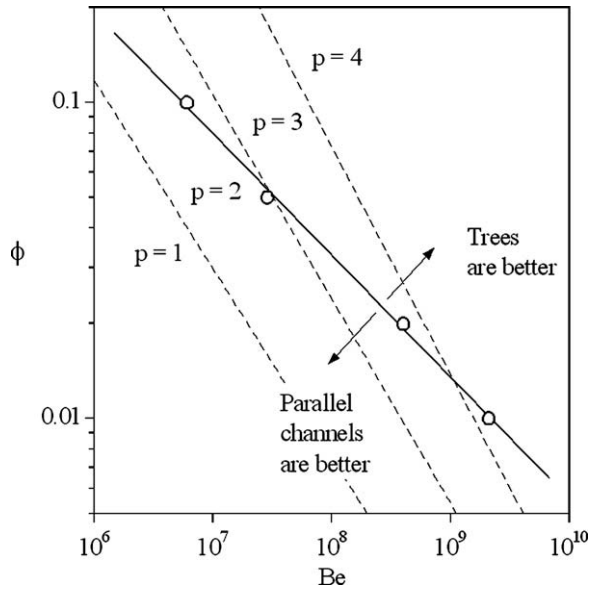

Fig. 11. Summary of the intersections of the envelopes (e.g., Figs. 6 and 9): the (ϕ,*Be*) domains in which trees and parallel channels are superior.

6. The area fraction occupied by high temperatures

The thermal performance evaluated and maximized up to this point was based on minimizing the temperature of the hot spots. To lower the temperature peaks means to decrease the overall temperature difference across the flow system, and this translates into decreasing the global thermal resistance of the cooling flow architecture.

When cooling is required in order to maintain the mechanical strength and physical integrity of the structure, low temperature peaks are not the only attractive thermal design feature. More important is to decrease the amount of material that is threatened by high temperatures. Here we propose to evaluate this aspect of thermal performance by defining the *hot volume fraction*

$$\sigma = \frac{V_\sigma}{V} \tag{25}$$

If T_{max} and T_{min} are the highest and lowest temperatures recorded in V, then there is a smaller volume (V_σ) that houses the points that have temperatures close to T_{max} but not equal to T_{max}. We chose V_σ such that the excess temperatures inside V_σ (namely $T_\sigma - T_{min}$) are greater than 90% of the largest excess temperature ($T_{max} - T_{min}$):

$$T_\sigma - T_{min} \geqslant 0.9(T_{max} - T_{min}) \tag{26}$$

In the present work, the volume is almost two-dimensional, so that instead of the volume ratio (25) we use the area ratio $\sigma = A_\sigma/A$. The area A is the area of a plane section parallel to the tree structure, for example the bottom (or top)-plane of an element (Fig. 2), where the hot spot occurs. An example is shown in Fig. 12. The smaller area (A_σ) is defined by the points with temperatures T_σ. The hot spot (T_{max}) is one point, which occurs in the upper-right corner. The hot-area (A_σ) is a layer (a two-dimensional volume) that forms "under the skin", i.e. under the surface exposed to intense heat flux. The hot layer is thicker in the vicinity of the hot spot, but that is not its only message. We learn from Fig. 12 that the tree structure used in the present designs could be bent optimally so that it might spread A_σ more uniformly under the wall. This direction of future development is sketched with dotted lines in Fig. 12.

On the basis of temperature fields such as Fig. 12, we evaluated σ as an alternative to $\tilde{T}_{max}$ for all the tree configurations presented in the preceding sections. The σ–*Be* alterative to Fig. 6 is presented in Fig. 13. For a given *Be* value, the hot-area fraction decreases sharply as the imposed pressure difference increases. The hot-area fraction is larger when the tree structure has more levels of bifurcation. Fig. 14 shows the same σ–*Be* trends for a lower porosity ($\phi = 0.02$): this figure is the counterpart of the $\tilde{T}_{max}$–*Be* results presented in Fig. 9.

An interesting view emerges when we combine the two evaluation methods, and plot $\tilde{T}_{max}$ versus σ for the same ϕ. For example, Fig. 15 was drawn by combining Figs. 6 and 13. This means that *Be* increases as the points slide down along each constant-*p* curve. Fig. 16 was drawn similarly, by combining Figs. 9 and 14.

Good thermal protection against intense heating from the side means that both low-$\tilde{T}_{max}$ and low-σ are attractive if they occur simultaneously. Figs. 15 and 16 tell us that this double objective is reachable more easily when the design relies on tree architec-

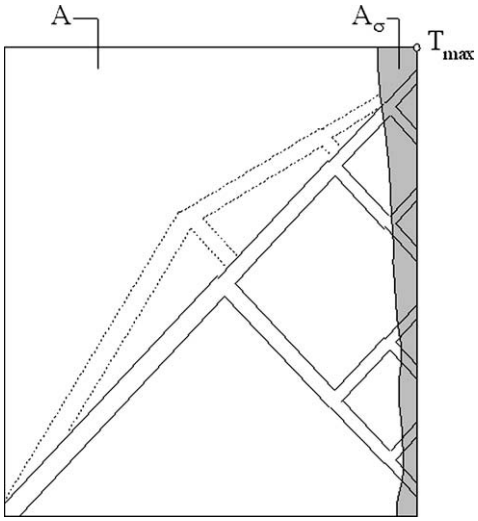

Fig. 12. Example of hot-area (A_σ) occurring in the bottom plane of a vascular design with $\phi = 0.02$, $p = 3$, and $Be = 10^8$.

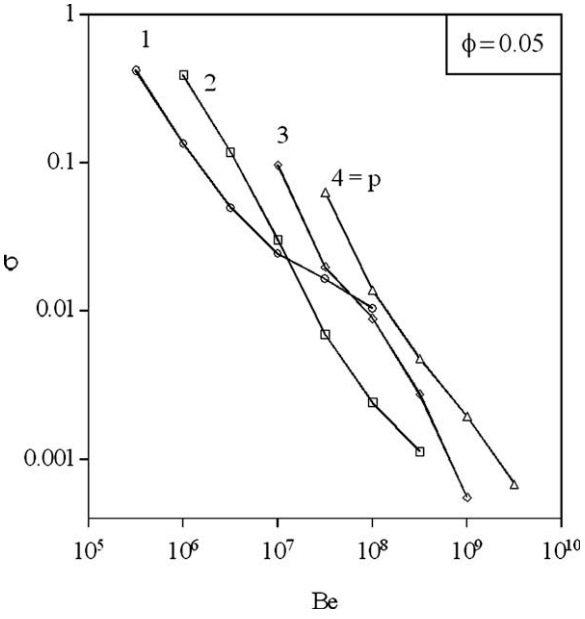

Fig. 13. The hot-area fraction σ for tree structures with $\phi = 0.05$.

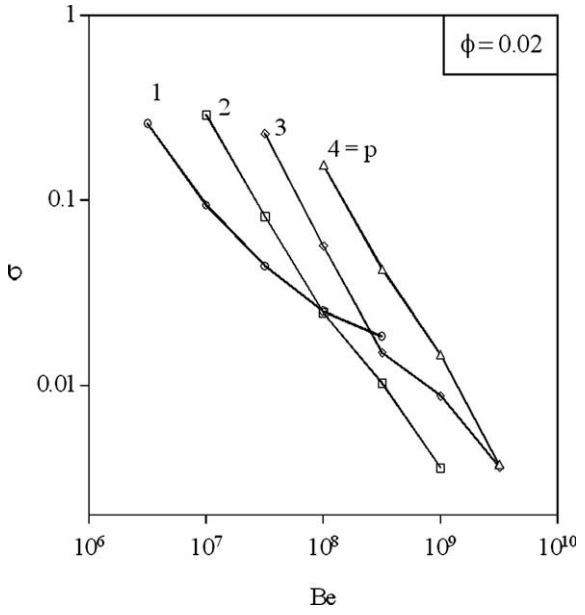

Fig. 14. The hot-area fraction σ for tree structures with $\phi = 0.02$.

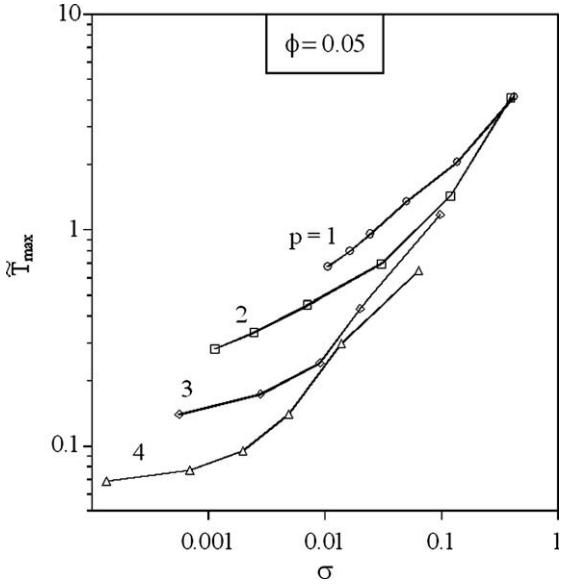

Fig. 15. Peak temperatures and hot-area fractions when $\phi = 0.05$.

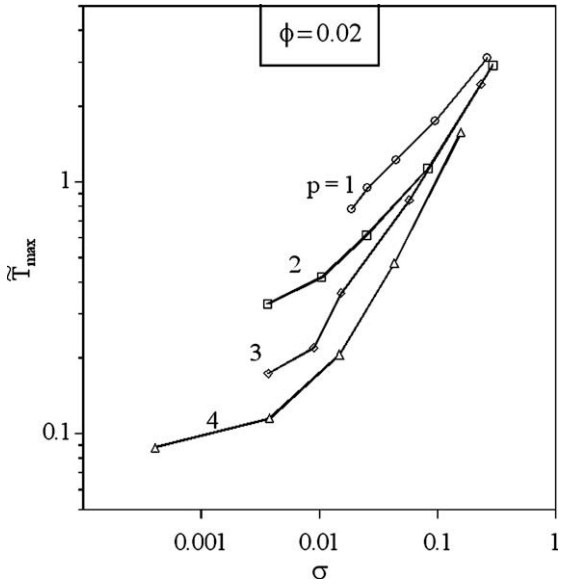

Fig. 16. Peak temperatures and hot-area fractions when $\phi = 0.02$.

tures with more levels of pairing (p). This is important to know, in addition to the earlier message about p conveyed by Fig. 11.

7. Flow resistance and pumping power

If the vascular design is deployed over the entire surface of a system that needs thermal protection against intense surface heating, then the pumping power required by the vasculature may be an important aspect to consider. Here we report the global fluid flow performance of the tree designs discussed until now from a thermal point of view.

The total mass flow rate ($\dot{m}_1$) driven by the imposed ΔP through the tree structure defined in Fig. 3 is represented by the dimensionless mass flow rate

$$\tilde{m} = \frac{\dot{m}_1}{Pr^{-1}\phi^2\mu L 2^{2p}/(2^p - 0.5)^4} \tag{27}$$

The pressure difference is represented by Be. The ratio $\tilde{m}/Be$ is the global conductance to fluid flow. Fig. 17 shows that the flow conductance is essentially constant when Be is small, and decreases when Be increases. This is another illustration of the effect of local pressure losses (e.g., Fig. 3), which become nonnegligible as Be and $\tilde{m}$ increase. The plateau exhibited by $\tilde{m}/Be$ in the low-Be limit is consistent with the low Reynolds number limit, where the overall ΔP is due to fluid friction distributed along the walls of the channels.

In summary, the global fluid flow performance is condensed in the value calculated for $\tilde{m}$ when Be, p and ϕ are specified. An alternative measure is the pumping power ($\dot{W} = \dot{m}_1 \Delta P/\rho$), which in dimensionless form is represented by the group

$$\widetilde{W} = \tilde{m}Be \tag{28}$$

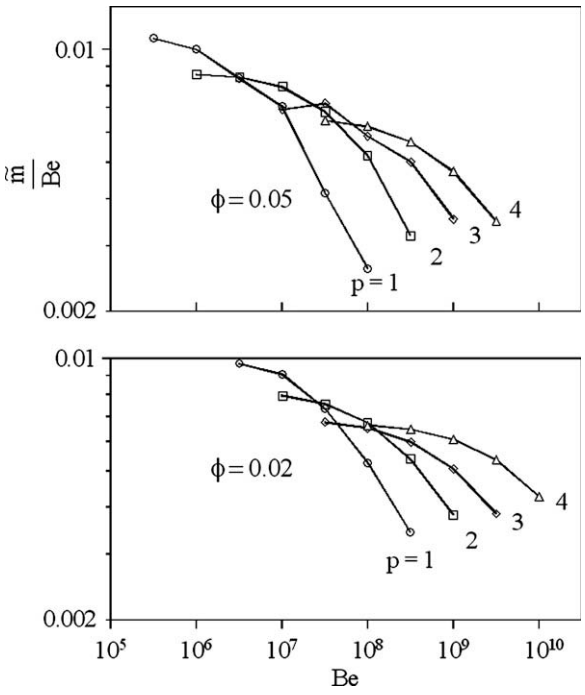

Fig. 17. The global fluid flow conductance of tree-shaped designs.

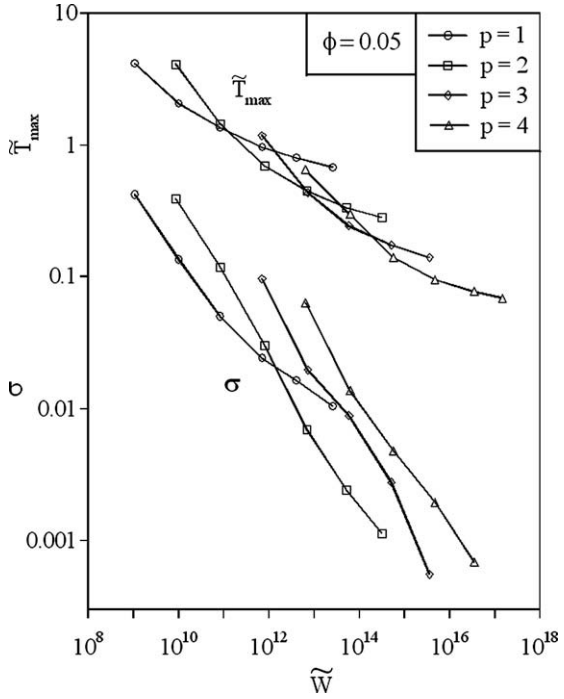

Fig. 18. Peak temperature and hot-area fraction versus pumping power.

Plots of flow conductance ($\tilde{m}/Be$), with $\tilde{W}$ on the abscissa look similar to Fig. 17, and are not shown. The curves of $\tilde{T}_{max}$ versus $\tilde{W}$ (Fig. 18) are similar to $\tilde{T}_{max}$ versus *Be* (Fig. 6). Fig. 18 also shows how the hot-area fraction varies when the pumping power is a parameter: the trends are the same as in Fig. 13. When the available pumping power increases, lower $\tilde{T}_{max}$ and σ can be achieved by using tree structures with more levels of pairing, i.e. finer structures.

8. Conclusions

In this paper, we investigated the merits of the proposal to vascularize a wall with transversal trees so that it can withstand intense heating from one side. The flow of the coolant through the tree vasculature is oriented against the wall. The hottest spots occur on the face that is exposed to intense heating; however, their temperature levels can be minimized through the selection of the type of tree architecture.

Comparisons with the thermal performance of corresponding configurations that use optimized parallel channels (oriented across the wall) showed that tree-shaped channels are more attractive than parallel channels when the imposed ΔP (or *Be*) and architecture porosity (ϕ) are large (Fig. 11). Parallel channels are the better performers when *Be* and ϕ are sufficiently small.

The existence of this "transition" between best configurations is a fundamental result because it is the essence of *technology evolution* [3]. Future research may determine how the transition line shifts as one ventures outside the domain covered by this study ($\tilde{k}, Pr, Be$), and as the flow regime in the channels changes. Trees, like parallel channels, are not for every application, and not for all scales. Because engineering always calls for the best flow architecture possible, the emerging flow configuration changes when the application and its size change. This conclusion is the key to solving the "scaling up" problem in engineering design [3].

Acknowledgements

This research was supported by the Air Force Office of Scientific Research based on a Grant for "Constructal Technology for Thermal Management of Aircraft". We thank Dr. David Moorhouse (Air Force Research Laboratory) for the advice and guidance that he gives us in this research direction.

References

[1] A. Bejan, Constructal-theory network of conducting paths for cooling a heat generating volume, Int. J. Heat Mass Transfer 40 (1997) 799–816.
[2] A. Bejan, Advanced Engineering Thermodynamics, second ed., Wiley, New York, 1997.
[3] A. Bejan, S. Lorente, Design with Constructal Theory, Wiley, Hoboken, 2008.
[4] A. Bejan, S. Lorente, Constructal theory of generation of configuration in nature and engineering, J. Appl. Phys. 100 (2006) 041301.
[5] A. Bejan, M.R. Errera, Convective trees of fluid channels for volumetric cooling, Int. J. Heat Mass Transfer 43 (2000) 3105–3118.
[6] D.V. Pence, Reduced pumping power and wall temperature in microchannel heat sinks with fractal-like branching channel networks, Microscale Thermophys. Eng. 6 (2002) 319–330.
[7] W. Wechsatol, S. Lorente, A. Bejan, Optimal tree-shaped networks for fluid flow in a disc-shaped body, Int. J. Heat Mass Transfer 45 (2002) 4911–4924.
[8] Y. Chen, P. Cheng, Heat transfer and pressure drop in fractal tree-like microchannel nets, Int. J. Heat Mass Transfer 45 (2002) 2643–2648.
[9] Y. Chen, P. Cheng, An experimental investigation on the thermal efficiency of fractal tree-like microchannel nets, Int. Commun. Heat Mass Transfer 32 (2005) 931–938.
[10] A.Y. Alharbi, D.V. Pence, R.N. Cullion, Fluid flow through microscale fractal-like branching channel networks, J. Fluids Eng. 125 (2003) 1051–1057.
[11] K.E. Enfield, J.J. Siekas, D.V. Pence, Laminate mixing in microscale fractal-like merging channel networks, Microscale Thermophys. Eng. 8 (2004) 207–224.
[12] X.-Q. Wang, A.S. Mujumdar, C. Yap, Numerical analysis of blockage and optimization of heat transfer performance of fractal-like microchannel nets, J. Electron. Packag. 128 (2006) 38–45.
[13] S.M. Senn, D. Poulikakos, Tree network channels as fluid distributors constructing double-staircase polymer electrolyte fuel cells, J. Appl. Phys. 96 (2004) 842–852.
[14] S.M. Senn, D. Poulikakos, Laminar mixing, heat transfer, and pressure drop in treelike microchannel nets and their application for thermal management in polymer electrolyte fuel cells, J. Power Sources 130 (2004) 178–191.
[15] A.K. da Silva, S. Lorente, A. Bejan, Constructal multi-scale tree shaped heat exchangers, J. Appl. Phys. 96 (2004) 1709–1718.
[16] A. Bejan, Dendritic constructal heat exchanger with small-scale crossflows and large-scales counterflows, Int. J. Heat Mass Transfer 45 (2002) 4607–4620.
[17] V.A.P. Raja, T. Basak, S.K. Das, Heat transfer and fluid flow in a constructal heat exchanger, in: R.K. Shah, M. Ishizuka, T.M. Rudy, V.V. Wadekar (Eds.), Proceedings of the Fifth International Conference on Enhanced, Compact and

Ultra-Compact Heat Exchangers: Science, Engineering and Technology, Engineering Conferences International, Hoboken, NJ, September 2005.
[18] V.A.P. Raja, Computational and experimental analysis of dendritic constructal heat exchanger, Doctoral Thesis, Indian Institute of Technology, Chennai, India, 2006.
[19] F. Lundell, B. Thonon, J.A. Gruss, Constructal networks for efficient cooling/heating, in: Proceedings of the Second Conference on Microchannels and Minichannels, Rochester, NY, 2004.
[20] M. Lallemand, F. Ayela, M. Favre-Marinet, A. Gruss, D. Maillet, P. Marty, H. Peerhossaini, L. Tadrist, Thermal transfer in microchannels: applications to micro-exchangers, in: French Congress on Thermics, SFT 2005, Reims, 30 May–2 June 2005.
[21] S. Kim, S. Lorente, A. Bejan, Vascularized materials: tree-shaped flow architectures matched canopy to canopy, J. Appl. Phys. 100 (2006) 063525.
[22] A. Bejan, S. Lorente, K.-M. Wang, Networks of channels for self-healing composite materials, J. Appl. Phys. 100 (2006) 033528.
[23] A. Aragón, C. Hansen, W. Wu, P. Geubelle, J. Lewis, S. White, Computational design and optimization of a biomimetic self-healing/cooling composite material, in: M.J. Dapino (Ed.), Behavior and Mechanics of Multifunctional and Composite Materials 2007, Proceedings of the Society of Photographic Instrumentation Engineers, vol. 6526, 2007, p. 65261G.
[24] S. Kim, S. Lorente, A. Bejan, Vascularized materials with heating from one side and coolant forced from the other side, Int. J. Heat Mass Transfer 50 (2007) 3498–3506.
[25] E. Weibel, Symmorphosis: On Form and Function in Shaping Life, Harvard University Press, Cambridge, MA, 2000.
[26] S. Lorente, W. Wechsatol, A. Bejan, Tree-shaped flow structures designed by minimizing path lengths, Int. J. Heat Mass Transfer 45 (2002) 3299–3312.
[27] S. Lorente, A. Bejan, Heterogeneous porous media as multiscale structures for maximum flow access, J. Appl. Phys. 100 (2006) 114909.
[28] STAR-CCM+ (Version 1.04) basics, CD-adapco Company.
[29] S. Bhattacharjee, W.L. Grosshandler, The formation of a wall jet near a high temperature wall under microgravity environment, ASME HTD 96 (1988) 711–716.
[30] S. Petrescu, Comments on the optimal spacing of parallel plates cooled by forced convection, Int. J. Heat Mass Transfer 37 (1994) 1283.
[31] S. Lorente, A. Bejan, Svelteness, freedom to morph, and constructal multi-scale flow structures, Int. J. Therm. Sci. 44 (2005) 1123–1130.